

Analysis of heat transport mechanisms from a Late Miocene model experiment with a fully-coupled atmosphere–ocean general circulation model

Arne Micheels^{a,b,*}, Angela A. Bruch^a, Jussi Eronen^{c,d}, Mikael Fortelius^{c,d,e}, Mathias Harzhauser^f, Torsten Utescher^g, Volker Mosbrugger^{a,b}

^a Senckenberg Research Institute and Natural History Museum, Senckenberganlage 25, D-60325 Frankfurt/Main, Germany

^b Biodiversity and Climate Research Centre (LOEWE BiK-F), Senckenberganlage 25, D-60325 Frankfurt/Main, Germany

^c Department of Geology, P.O. Box 64, FIN-00014 University of Helsinki, Finland

^d Department of Computer Sciences, P.O. Box 64, FIN-00014 University of Helsinki, Finland

^e Department of Geology and Institute of Biotechnology, P.O. Box 64, FIN-00014 University of Helsinki, Finland

^f Geological-Paleontological Department, Natural History Museum Vienna, Burgring 7, A-1010 Vienna, Austria

^g Geological Department, University of Bonn, Nuffallee 8, D-53115 Bonn, Germany

ARTICLE INFO

Article history:

Received 31 August 2009

Received in revised form 28 June 2010

Accepted 20 September 2010

Available online 16 October 2010

Keywords:

Climate modelling

Atmosphere–ocean general circulation model

Neogene

Miocene

Heat transport

ABSTRACT

The fossil record for the Late Miocene indicates that high latitudes were warmer than today and that the equator-to-pole temperature gradient was weak. Experiments with climate models have not been sufficiently able to represent warm polar conditions for the Late Miocene. This demonstrates that our explanation of warm high latitudes in the Late Miocene is not complete. In addition, heat transport mechanisms have not been so frequently addressed to understand the differences between the Late Miocene and modern climate. Here we present a model simulation for the Tortonian (11 to 7 Ma) using a complex fully-coupled atmosphere–ocean general circulation model to address heat transport mechanisms relative to modern conditions. Because of an open Central American Isthmus, the zonal mean northward ocean heat transport in the Northern Hemisphere generally decreases in our Tortonian run. As a consequence, the northward atmospheric heat transport is stronger in the Tortonian experiment. In northern mid-latitudes, the sensible and latent heat fluxes related to transient eddies increase compared to today. The stronger poleward transient eddy heat transport in the Tortonian model run correlates with intensified stormtracks in the mid-latitudes. In the palaeoclimate model run, the increased northward transient eddy heat transport together with the different-than-present land surface cover leads to a warming of polar regions and, hence, to a reduction of the meridional temperature gradient. The low elevation of Tibet in our palaeoclimate experiment causes a general weakening of the monsoon system in Asia. The E-Asian monsoon precipitation decreases compared to our reference run, but monsoon rainfall in India increases. When comparing the model results with quantitative terrestrial proxy data, we observe some discrepancies for some specific localities. However, the large patterns in our Tortonian run agree fairly well with the fossil record.

© 2010 Elsevier B.V. All rights reserved.

1. Introduction

Even though the Miocene (23 to 5.3 Ma) belongs to the late phase of the Cenozoic climate cooling, it was still characterised by warm and humid climatic conditions compared to today (e.g., Wolfe, 1994a,b; Zachos et al., 2001, 2008; Mosbrugger et al., 2005; Fauquette et al., 2007; Liu et al., 2011-this issue; Yao et al., 2011-this issue). Marine evidences support that tropical sea surface temperatures were warmer than present in the Early to Middle Miocene (e.g., Stewart et al., 2004). Following the general climate

cooling trend (e.g., Zachos et al., 2008), equatorial regions were as warm as today in the Late Miocene (Williams et al., 2005; Steppuhn et al., 2006) and in the Pliocene the tropics appeared to be even cooler than at present (Dowsett, 2007). Particularly polar regions were warmer in the Miocene (e.g., Wolfe, 1994a,b). Palaeobotanical data suggest that the Late Miocene in Siberia was much warmer compared to today (Utescher et al., 2011-this issue). Similarly for the North Pacific in the Late Miocene, marine evidences indicate warm conditions compared to today (Lyle et al., 2008, and references therein). Therefore, the equator-to-pole temperature gradient was relatively weak (e.g., Crowley, 2000; Fauquette et al., 2007). In the Miocene, the Alps just started to form (e.g., Kuhlemann, 2007), and the uplift of the Tibetan Plateau continued (e.g., Molnar, 2005). The Central American Isthmus was open in the Miocene (e.g., Collins et al., 1996; Bartoli et al., 2005), and the meridional overturning

* Corresponding author. Senckenberg Research Institute and Natural History Museum, Senckenberganlage 25, D-60325 Frankfurt/Main, Germany.

E-mail address: arne.micheels@senckenberg.de (A. Micheels).

circulation in the North Atlantic Ocean was weaker than today (e.g., Mikolajewicz and Crowley, 1997; You et al., 2009). There were some differences, but the global continent configuration in the Miocene (e.g., Herold et al., 2008) was largely comparable to the modern situation. Hence, the Miocene represents a general hothouse situation and because of its similarities it can serve as a possible analogue for the future climate change (e.g., Kutzbach and Behling, 2004; Micheels et al., 2009b).

Climate modellers focussed on the Miocene to understand the relevant climate processes (e.g., Maier-Reimer et al., 1990; Dutton and Barron, 1997; Mikolajewicz and Crowley, 1997; Ramstein et al., 1997; Ruddiman et al., 1997; Bice et al., 2000; Liu and Yin, 2002; Kutzbach and Behling, 2004; Steppuhn et al., 2006, 2007; Micheels et al., 2007, 2009a,b; Lunt et al., 2008; You et al., 2009). Thereby, modelling studies using atmospheric general circulation models (AGCMs) either with prescribed sea surface temperatures or slab ocean models frequently favoured the analysis of the uplift of the Tibetan Plateau and its influence on the evolution of the Asian monsoon (e.g., Ramstein et al., 1997; Fluteau et al., 1999; Liu and Yin, 2002). Using AGCMs coupled to slab ocean models, sensitivity experiments also concentrated on different concentrations of atmospheric CO₂ in the Miocene (Steppuhn et al., 2007; Micheels et al., 2009b; Tong et al., 2009), and on the climatic effects of the palaeovegetation (Dutton and Barron, 1997; Micheels et al., 2009a). Sensitivity experiments with ocean general circulation models (OGCMs) for the Miocene repeatedly addressed the opening and closure of ocean gateways (e.g., Mikolajewicz and Crowley, 1997; Bice et al., 2000; Nisancioglu et al., 2003; von der Heydt and Dijkstra, 2006). These studies demonstrated that the open Panama Isthmus in the Miocene led to a weaker-than-present meridional circulation in the North Atlantic and, hence, to a reduced northward ocean heat transport (e.g., Mikolajewicz and Crowley, 1997; Bice et al., 2000; Nisancioglu et al., 2003; von der Heydt and Dijkstra, 2006). Steppuhn et al. (2006) used an AGCM coupled to slab ocean model to analyse the Late Miocene atmospheric response on a weaker-than-present ocean heat transport. Lunt et al. (2008) considered different scenarios for Late Miocene sea surface temperatures (SSTs) to identify regions with pronounced climatic differences between the Late Miocene and today.

There exist a number of climate model experiments for Miocene time intervals. However, climate model experiments were not able to describe sufficiently warm polar conditions compared to Miocene proxy data (Steppuhn et al., 2006, 2007; Micheels et al., 2007). It remains enigmatic to understand warm high latitudes, if e.g. the northward heat transport in the North Atlantic Ocean was weak. How can we understand the weaker-than-present meridional temperature gradient in terms of heat transport mechanisms? In a sensitivity study, Micheels et al. (2009a) investigated the climate response on the appearance of the modern Sahara desert in the Late Miocene. They found that the appearance of the Sahara desert led to cooling in higher latitudes because of modifications in the atmospheric heat transport. However, Micheels et al. (2009a) used a simple AGCM coupled to a slab ocean model with a present-day flux correction. Ocean model experiments have not yet properly specified atmospheric forcing for Miocene conditions (e.g., Mikolajewicz and Crowley, 1997; Bice et al., 2000). Miocene model experiments using fully-coupled atmosphere–ocean general circulation models (AOGCMs) are lacking, but they are required to understand the coupled system of atmosphere and ocean.

In the present study, we apply a fully-coupled atmosphere–ocean general circulation model to the Tortonian (Late Miocene, 11 to 7 Ma). Our Tortonian AOGCM sensitivity experiment aims to analyse the heat transport mechanisms. We compare the total atmospheric heat transported with the total ocean heat transport (Tortonian versus present-day). We further describe atmospheric heat fluxes associated with the mean meridional circulation and with transient and stationary eddies, and the respective fluxes of potential energy and sensible and latent heat. Details on the ocean circulation are beyond

the scope of the present paper. We set special emphasis on the atmospheric patterns of our Tortonian run, not the least because we use quantitative terrestrial proxy data to test the reliability of the model results.

2. Model description and experimental design

2.1. The COSMOS model

For our model experiments for the Late Miocene, we use the atmosphere–ocean general circulation model COSMOS (e.g., Roeckner et al., 2003, 2006; Jungclaus et al., 2006). This fully-coupled AOGCM was developed at the Max Planck Institute for Meteorology in Hamburg (Germany). It is one of the most recent highly complex climate models, which has been used for future climate change projections (Meehl et al., 2007). The atmosphere model of COSMOS is ECHAM5 (Roeckner et al., 2003). The horizontal resolution of the spectral AGCM is T31, which corresponds to a Gaussian grid of 3.75°×3.75° in longitude and latitude. The vertical domain is represented by 19 layers using terrain-following hybrid σ -coordinates. The integration time step for the atmosphere model is 30 min. ECHAM5 is based on the primitive equations. Atmospheric dynamics are formulated in spherical harmonics, whereas non-linear terms are formulated in the grid point space. ECHAM5 includes parameterisations of various physical processes such as for radiation transfer, convection and horizontal diffusion. The radiation transfer scheme considers trace gases such as carbon dioxide. Atmospheric CO₂ is specified with 360 ppm in our present-day control experiment (referred to as CTRL in the following). For practical reasons, the radiation transfer scheme has an integration time step of 2 h. The model version used in the present study does not include a dynamical vegetation model. Vegetation is a fixed factor represented by specifying different land surface parameters like albedo, roughness length and maximum soil water capacity (Hagemann, 2002). Further technical details of the atmosphere model ECHAM5 are described in the model documentation (Roeckner et al., 2003).

The ocean model of COSMOS is MPIOM (Marsland et al., 2003), which is an advanced version of the OGCM HOPE (Wolff et al., 1997). MPIOM uses an Arakawa-C grid with an approximate resolution of 3°×3° in the horizontal plane. The orthogonal curvilinear Arakawa grid has its two poles in Greenland and in the centre of Antarctica. The vertical domain is represented by 40 unevenly spaced layers. The integration time step is 144 min. MPIOM is based on the primitive equations for a hydrostatic Boussinesque fluid with a free surface. The ocean model parameterises several physical processes. For instance, MPIOM parameterises isopycnal tracer mixing by unresolved eddies using the Gent-McWilliams scheme (Gent et al., 1995). The vertical eddy viscosity and diffusion parameterisation scheme is based on Pacanowski and Philander (1981), but modified to better represent turbulent mixing near the surface. For further details of the ocean model, we refer to the model documentation (Marsland et al., 2003).

2.2. The Late Miocene configuration

We perform a model experiment with COSMOS for the Tortonian (11 to 7 Ma, Late Miocene). The Tortonian run is referred to as TORT in the following. The model setup of TORT is largely based on previous studies for the Late Miocene using the AGCM ECHAM4 coupled to a slab ocean model (Steppuhn et al., 2006, 2007; Micheels et al., 2007). For ECHAM5, the palaeogeography, the palaeogeography, the palaeovegetation, the CO₂ concentration and the orbital parameters need to be adapted; MPIOM requires modifications of the palaeogeography and the palaeobathymetry.

The land–sea distribution (Fig. 1) of TORT is largely the same as today because the relatively coarse model resolution does not allow for the representation of details. Australia was farther south in

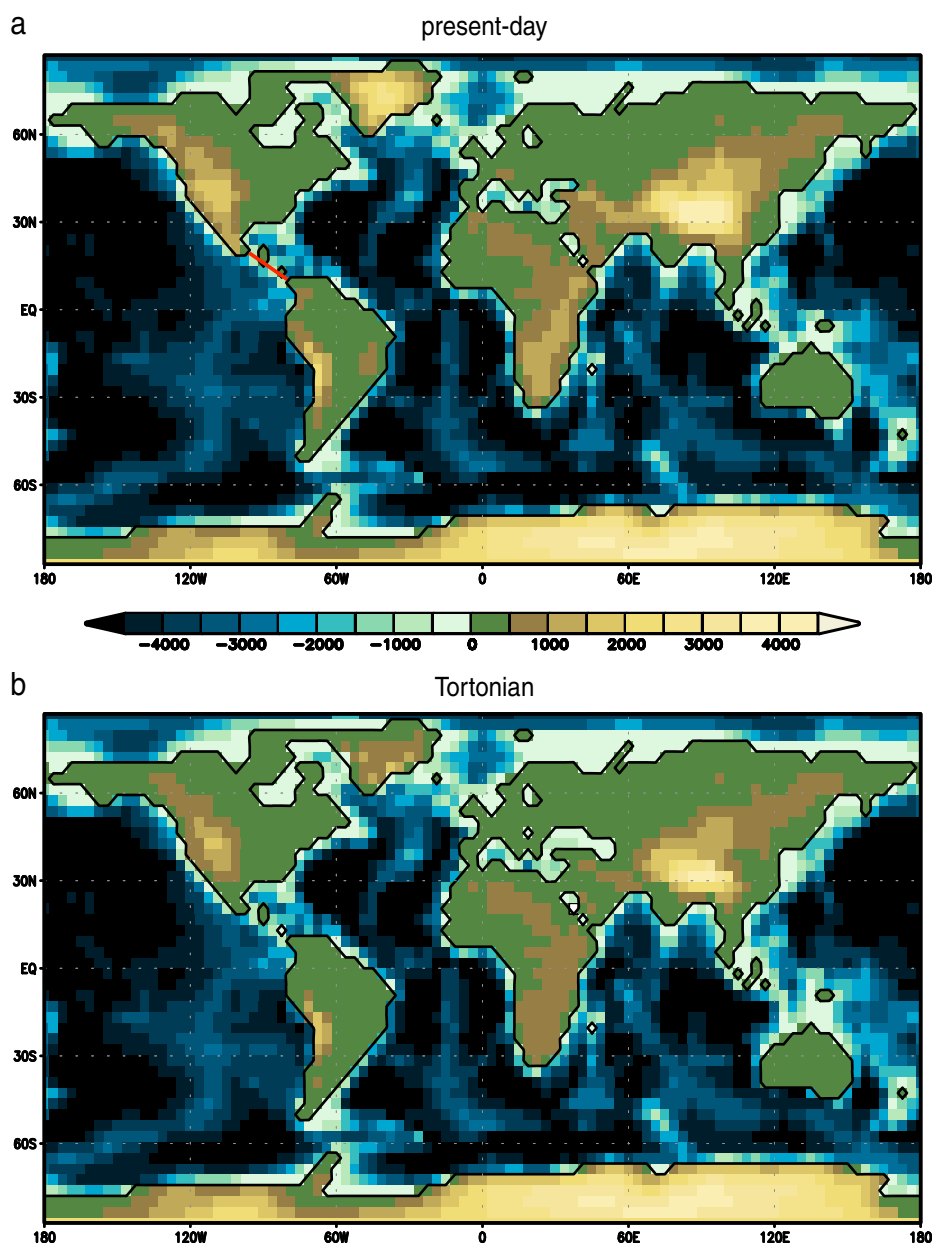


Fig. 1. The land–sea distribution (contour lines), the orography and bathymetry (in m) of a) the present-day control run, and b) the Tortonian run. The red bar in a indicates that in the ocean model the Atlantic and Pacific Ocean are not connected in the present-day control run (see text for details).

the Miocene (e.g., Lawver and Gahagan, 2003; Herold et al., 2008), and we moved Australia two grid cells southward in TORT compared to CTRL. We include the Paratethys (based on Harzhauser and Piller, 2007; Popov et al., 2004; Rögl, 1998) and the Pannonian Lake (based on Harzhauser and Mandic, 2008; Magyar et al., 1999). Fig. 1b illustrates that the Paratethys is a shallow sea compared to the Mediterranean basin. No reliable depth estimates are available for this area and time slice to date. Nevertheless, based on facies descriptions and scarce faunistic data, a general model is depicted, which serves as a satisfactory base for our modelling purposes. The northern part of the Eastern Paratethys is a shallow sea with an average depth of about 100 metres, while the more southern part of the basin reaches depths of up to 1000 metres (cf. Popov et al., 2004). The Pannonian Lake, with a water surface of 290,000 km² has a depth of up to 500 metres, although larger parts have been much shallower (Magyar et al., 1999; Harzhauser and Mandic, 2008). A major characteristic of the Miocene is the open Central American Isthmus. Due to the model resolution,

the present-day land–sea distribution (Fig. 1a) of the atmosphere model seems to represent an open gateway, but it is closed for the ocean model. The ocean configuration of TORT considers an open Panama gateway with a depth of 500 metres (based on Collins et al., 1996), although the land–sea distribution of the atmosphere model is the same as in CTRL (Fig. 1b).

Related to geographic differences between the Late Miocene and present, we adapt the orography (Fig. 1). The palaeorography is basically lower in TORT compared to CTRL. For instance, we consider that the mean elevation of the Tibetan Plateau is about 70% of the modern height. Spicer et al. (2003) suggested that the most southern part of Tibet was as high as today over the last 15 Ma, but the mean elevation of Tibet was lower than today (Molnar, 2005). Greenland is also much lower than today because we remove the modern ice sheet. The Alps started to form in the Oligocene and were still low in the Miocene (e.g., Spiegel et al., 2001; Kuhlemann, 2007). In TORT, they are reduced to about 70% of its present-day elevation.

We use a proxy-based reconstruction of the Tortonian vegetation (Micheels et al., 2007). The Late Miocene vegetation is characterised by a larger-than-present forest cover and less deserts (Fig. 2). Boreal forests extend far more towards the high latitudes and cover regions where we find tundra or even polar desert today. In low latitudes, rainforests are more widespread in TORT than in CTRL. The present-day desert areas are grass- to shrublands in the Tortonian run. In particular, there is no Sahara desert in North Africa but grassland to savannah vegetation cover in TORT. Le Houerou (1997) suggested that there was no desert in North Africa before the Pliocene, whereas Senut et al. (2009) stated that the Sahara desert appeared already at around 8 to 6 Ma, most likely at 7 to 6 Ma. Swezey (2009) proposed sufficiently high precipitation for fluvial systems in the Late Miocene. Hence, evidences from the fossil record (e.g., Le Houerou, 1997; Pickford, 2000; Jacobs, 2004; Swezey, 2009) support rather more grassland vegetation than desert in North Africa in the Tortonian (11 to 7 Ma).

We specify orbital parameters with the present-day default values because the Tortonian covers a time span of 4 million years including several orbital cycles. Atmospheric carbon dioxide concentration is set to 360 ppm. This value is reasonable for the Late Miocene (e.g., Pearson and Palmer, 2000; MacFadden, 2005; Pagani et al., 2005; Micheels et al., 2007, 2009b) and it is also the same as in our present-day control experiment. Except for the boundary conditions described above, all other configurations in TORT remain the same as in CTRL. Both the Tortonian and the control run are integrated over 2500 years to ensure that the model is in its dynamic equilibrium. The last 10 years are used for our further data analysis. In the following section, we first describe anomaly patterns of temperature and precipitation between the Tortonian run and the present-day reference experiment. Then, we focus on heat transport mechanisms to understand differences between the Tortonian and modern climate situation. In order to evaluate the reliability of these model results, we finally perform a comparison of TORT with quantitative terrestrial proxy data.

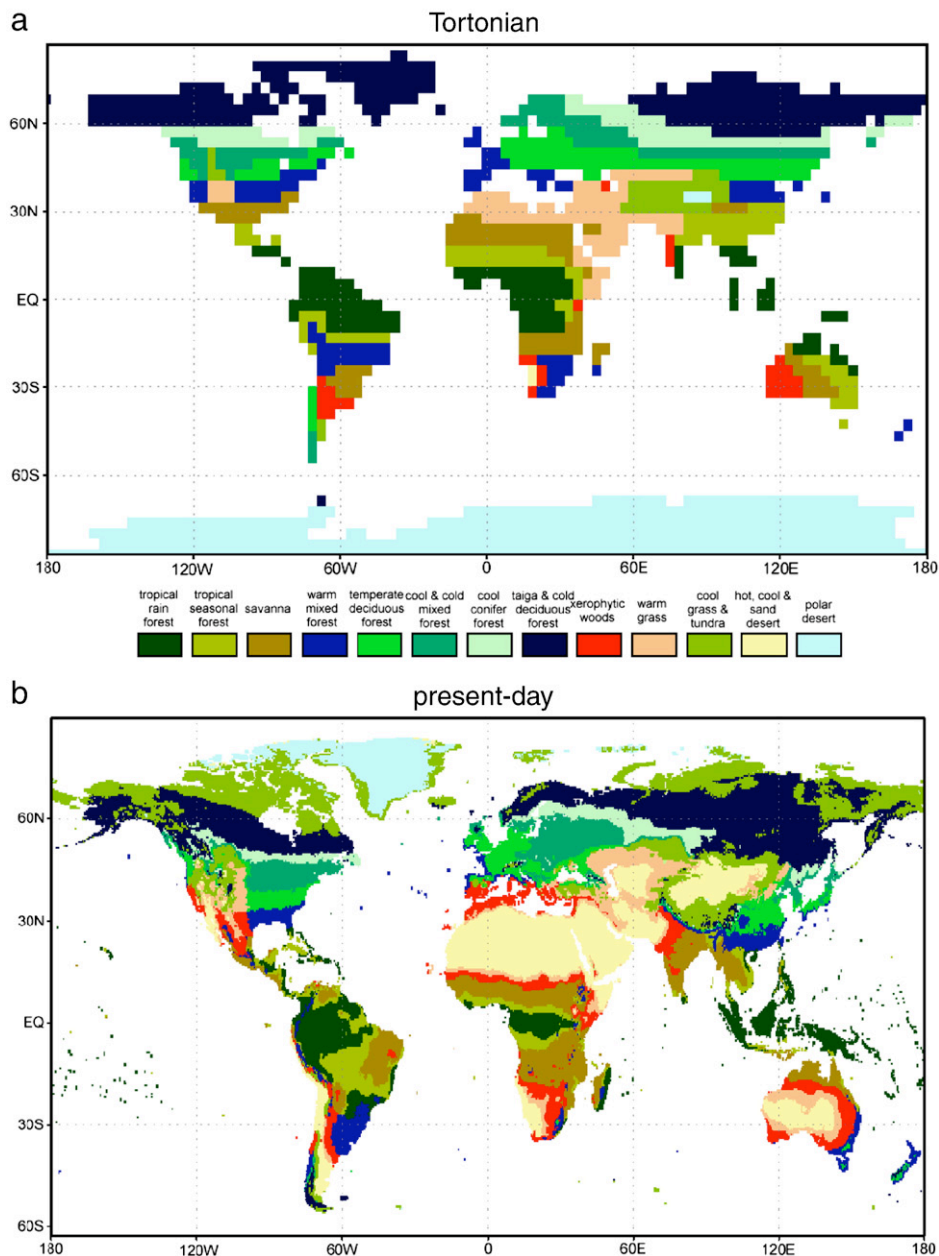


Fig. 2. a) The proxy-based palaeobotanical reconstruction of the Tortonian vegetation, and b) the present-day vegetation calculated from a biome model (from Micheels et al., 2007).

3. Results

3.1. The Tortonian run compared to the control run

The Tortonian run represents globally warmer and wetter conditions than the present-day control run. The global temperature in TORT (18.0 °C) is +1.5 °C higher than in CTRL (16.5 °C), and global precipitation increases by +43 mm/a in TORT (1110 mm/a) compared to CTRL (1067 mm/a). As a result of global warming in TORT, the sea ice volume is largely reduced from $8.5 \times 10^{12} \text{ m}^3$ in CTRL to $4.4 \times 10^{12} \text{ m}^3$ in TORT, which is about the half (−48%). Fig. 3a indicates that the zonal average temperatures are generally elevated by +1 °C to +2 °C in the Tortonian experiment. In the high latitudes, there is a pronounced warming, which can be attributed to the lower elevation of Greenland and the reduced sea ice in TORT. Hence, the meridional temperature gradient is by about −2 °C weaker than in CTRL. At around 60 °N, zonal average temperatures in TORT still represent a warming, but with less than +1 °C it is less pronounced than in all other latitudes.

The warming in TORT compared to CTRL correlates with a positive difference in the net radiation flux at the surface (Fig. 3b). The net surface radiation flux between both runs represents a distinct peak at 15 °N to 30°N, which indicates that (amongst others) the Tortonian grassland to savannah vegetation instead of the modern Sahara desert (cf. Fig. 2) leads to a higher energy input via the albedo effect. Similarly, the vegetation differences in Greenland and the reduced amount of sea ice in TORT contribute to an increase in the surface radiation flux. The effect in high latitudes is relatively stronger than in equatorial regions because absolute values of the radiation flux are much less. Overall, the energy input in the Earth's system is higher than today and, therefore, temperatures increase in the Tortonian experiment.

Fig. 4a illustrates a significant warming in higher latitudes of TORT compared to CTRL, but also low and mid-latitudes are warmer. The warming in TORT is most pronounced in Greenland, over the Tibetan Plateau, and in North Africa. For Greenland and Tibet, the lowering of the elevation (cf. Fig. 1) leads to temperature increases of more

than +10 °C compared to modern conditions. Reduced elevations in other mountain areas (e.g., southern Africa, the Andes) also cause higher temperatures in TORT. However, these warming effects are less because reductions of orography are smaller than for Greenland and Tibet. The strong temperature increase in Greenland is also due to the different vegetation cover (cf. Fig. 2). The albedo effect (boreal forest instead of the modern Greenland ice sheet) contributes to the heating effect of the reduced surface elevation. Similarly in North Africa, the lower albedo of the Tortonian grassland to savannah vegetation compared to the modern Sahara desert leads to a pronounced warming of up to +6 °C in TORT compared to CTRL.

In contrast to the overall warmer conditions in TORT, the North Atlantic and European region tends to be cooler than CTRL (Fig. 4a). Over the North Atlantic cooling is most pronounced with −2 °C and N-Europe is about −1 °C cooler. Central Europe is (more or less) as warm as today in TORT and the Mediterranean is about +2 °C warmer following the global trend. The cooling in the North Atlantic/European region is a result of the open Central American Isthmus in the Tortonian run, which causes a weaker northward heat transport in the Atlantic Ocean (see below).

Focusing on precipitation (Fig. 4b), most regions in TORT represent more humid conditions than today. In the warm Tortonian run, generally more water evaporates from the Earth's surface (including transpiration of vegetation), which enhances precipitation. For instance, annual precipitation in Africa strongly increases (up to +2 mm/day) compared to the reference run. Temperatures close to the equator in Africa (Fig. 4a) do not change much compared to the centre of North Africa. This is because in TORT evaporative cooling, related to increased rainfall, dampens the albedo effect. In tropical equatorial regions, precipitation in TORT is greater than in CTRL. Rainfall contrarily decreases in the subtropics of the eastern Pacific Ocean. There, intensified trade winds in TORT transport more moisture from subtropical into tropical regions. From the North Atlantic Ocean towards Europe, precipitation rates increase because of an increased moisture flux with the westerlies in TORT. In Asia, precipitation in TORT increases over India and SE-Asia, whereas E-Asia is drier than CTRL. The lower palaeoelevation of Tibet and the warm Indian Ocean intensify the Indian and SE-Asian monsoon rainfall in TORT. Contrarily the E-Asian monsoon precipitation is weaker than today.

3.2. Heat transport mechanisms

In order to understand climatic differences between TORT and CTRL described above, we need to focus on heat transport mechanisms (Fig. 5). Fig. 5a illustrates the total atmospheric heat transport (AHT) and the ocean heat transport (OHT). Pronounced differences in heat transport between TORT and CTRL occur in the Northern Hemisphere, whereas changes are smaller in the south. As expected, the open Central American Isthmus in TORT leads to a weaker northward ocean heat transport than in CTRL. The OHT difference peaks at around 30 °N with a maximum reduction of −0.5 PW. Compensating for the weaker-than-present ocean heat transport, the northward atmospheric heat flux is generally enhanced in TORT. The difference of the AHT between both experiments has an almost bimodal shape with pronounced peaks at 10 °N (+0.5 PW) and at 30 °N (+1 PW). The northern peak correlates with the latitudinal position of Tibet and North Africa. From 30 °N to 45 °N, the atmospheric heat flux difference strongly declines resulting in a (slightly) reduced northward transport in TORT than in CTRL. Hence, the atmosphere cannot compensate for the weakened ocean heat transport (related to the open Central American Isthmus) and we observe a cooling over the North Atlantic region (Fig. 4a).

The total heat transport (e.g., $\overline{v \cdot T}$ in case of the sensible heat flux) is split up into proportions which belong to the mean flow ($\overline{v} \cdot \overline{T}$), stationary ($\overline{v' \cdot T^*}$) and transient eddies ($\overline{v' \cdot T'}$) (Fig. 5b). There are small reductions of the stationary eddy heat transport in TORT at

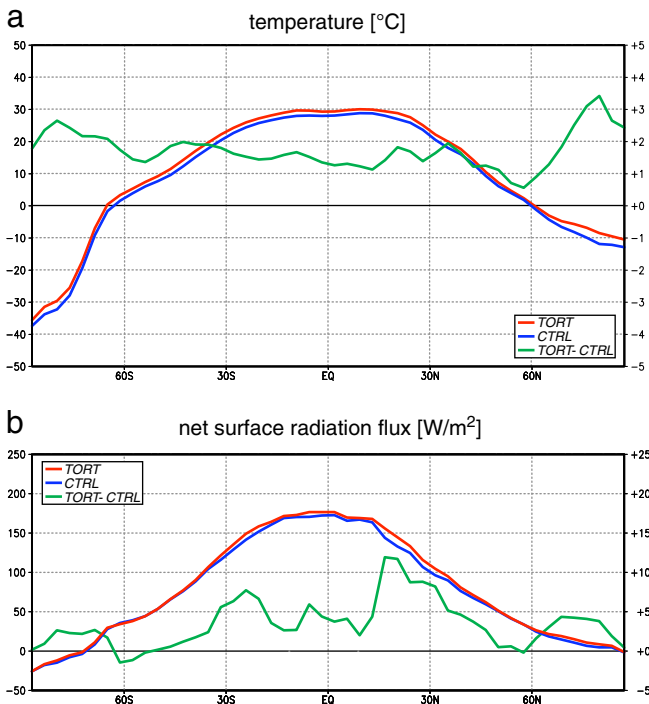


Fig. 3. The zonal averages of a) temperature (in °C), and b) net surface radiation flux (in W/m²) of TORT (red), CTRL (blue), their differences (green). The left scales refer to absolute values and right scales refer to differences.

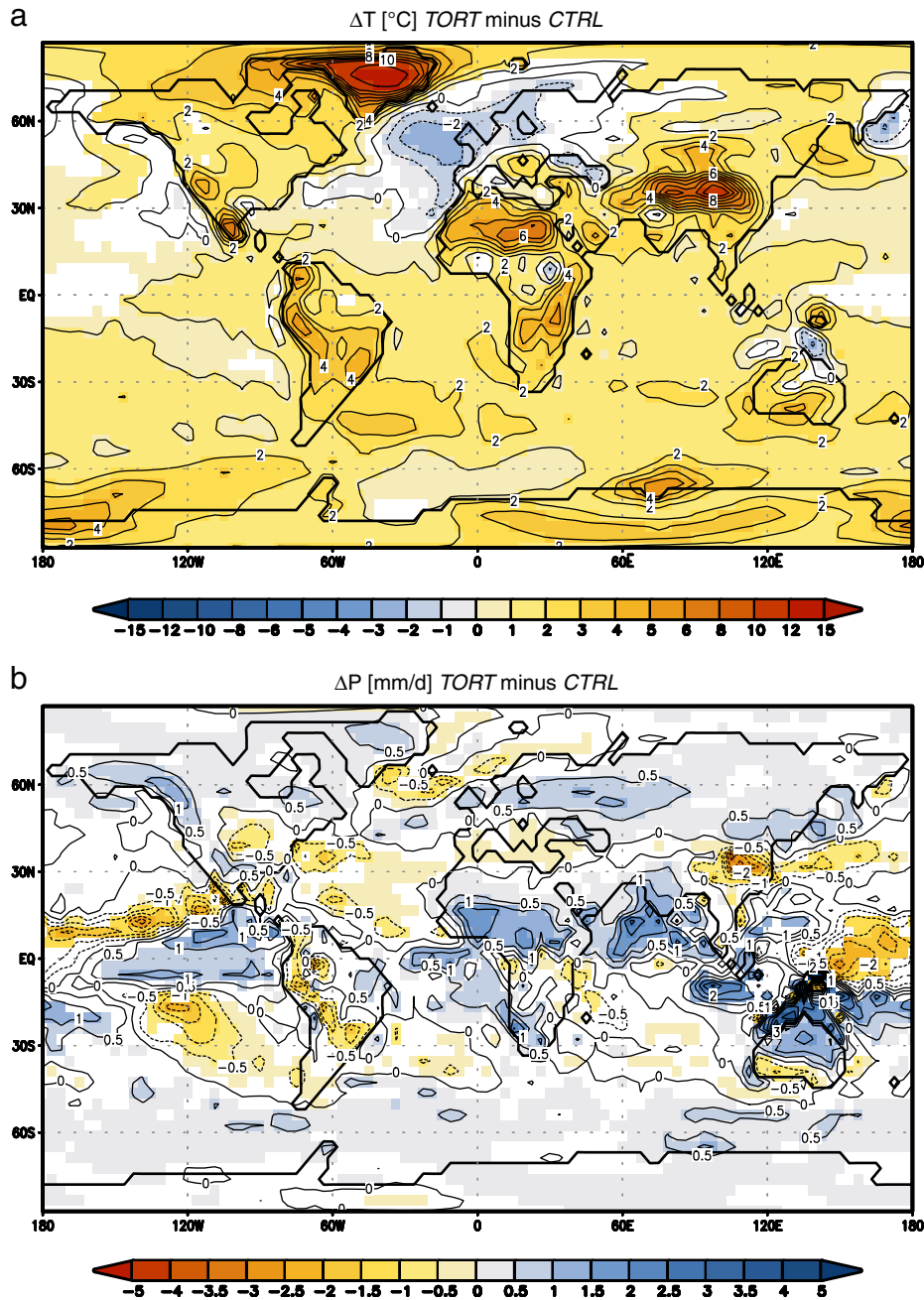


Fig. 4. The annual average differences for a) temperature (in °C), and b) precipitation (in mm/day) between the Tortonian and the present-day control run. Non-coloured white areas represent non-significant anomalies with a Student's *t*-test ($p = 0.05$).

around 30 °N and 60 °N, which are consistent with the reduced palaeoelevation of Tibet and Greenland (Fig. 1). However, differences in stationary eddy heat transport between TORT and CTRL are negligible compared to the mean flow and transient eddies. From 15 °N to 60 °N, the poleward transient eddy heat transport gets stronger in TORT (+0.4 PW). This indicates that the atmosphere compensates for the reduced heat transport in the North Atlantic (Fig. 5a) in TORT with more frequent/intense storms than in CTRL. Fig. 6 illustrates the stormtracks, i.e. the variance of the band-pass filtered geopotential field at 500 hPa. In TORT, the stormtracks over the northern Pacific and Atlantic Ocean are much more intense than in the control experiment. The most pronounced changes in stormtrack activity occur over the continental areas between 40 °N and 60 °N. Particularly north-east of the Paratethys, there is a local maximum in TORT (Fig. 6a), which is hardly represented in CTRL (Fig. 6b). The increased

stormtrack activity in this area is associated with a locally increased temperature gradient in TORT since the presence of the Paratethys leads to a warming effect in the winter season.

Comparing Fig. 5a and b, the mean flow heat transport is, however, the dominating factor to understand differences between TORT and CTRL. The AHT differences observed from Fig. 5a are mostly a result of modifications of the heat transport with the atmospheric mean meridional circulation (Fig. 5b). The increased heat transport out of tropical latitudes into the northern mid-latitudes is realised by the mean flow (cf. Fig. 5a). In contrast, the heat transport with the mean meridional circulation is reduced in the northern mid-latitudes (−0.5 PW) in TORT.

Fig. 5c illustrates the amount of energy which is transported in the atmosphere in form sensible, potential and latent heat. Changes in the mean flow heat flux (Fig. 5b) correlate with the differences in the

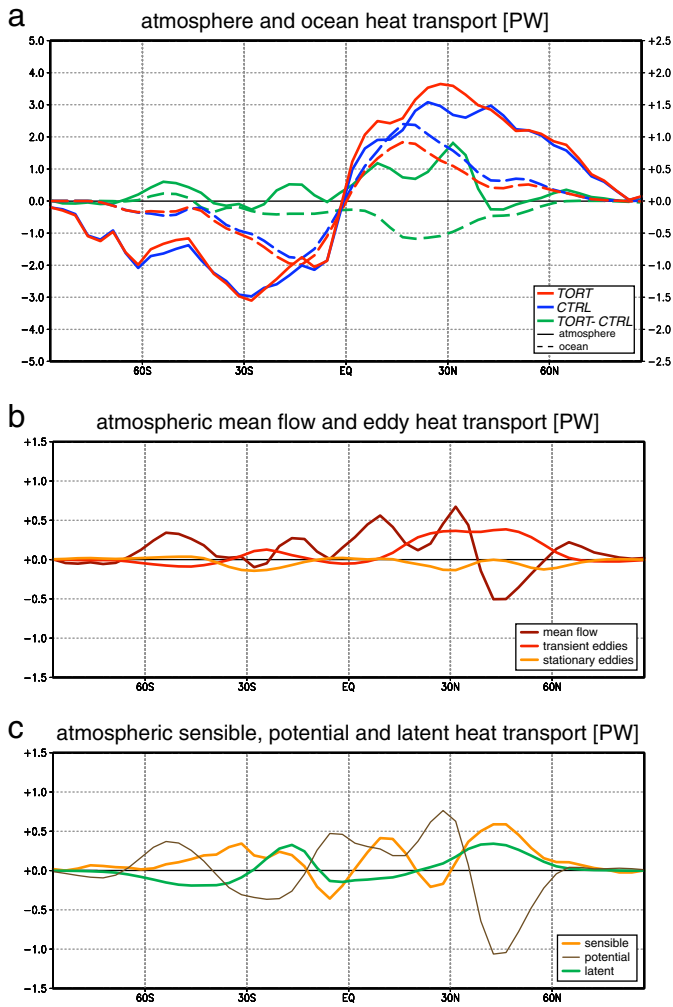


Fig. 5. The vertically and zonally integrated time averages of a) the atmospheric (solid) and oceanic (dashed) heat transport (in PW) of the Tortonian run (red), the present-day control run (blue), and their differences (green), b) the differences in the atmospheric mean flow (dark red), transient eddy (red) and stationary eddy (orange) heat transport (in PW) between TORT and CTRL, and c) the differences in the atmospheric latent (green), sensible (orange) and potential (brown) heat transport (in PW) between TORT and CTRL. The left scale in a refers to absolute values and the right scale refers to differences, in b and c the left scales refer to differences.

potential energy transport. In the low latitudes, the increased northward heat flux (Fig. 5a) with the mean flow (Fig. 5b) in TORT is a result of the intensified potential heat flux. In northern mid-latitudes, the poleward potential heat transport is much weaker (−1 PW) than in CTRL. Mostly, this is due to a reduced potential energy transport within the mean flow (Fig. 5b). In the lower latitudes, there tends to be stronger northward sensible heat flux (Fig. 5c) in TORT, whereas the latent heat flux slightly decreases compared to CTRL. Proceeding farther towards northern mid-latitudes, the poleward sensible (+0.5 PW) and latent (+0.4 PW) heat fluxes increase (Fig. 5c), which is primarily realised by transient eddies but also by the mean meridional circulation (Fig. 5b). The position of increases in the sensible and latent heat fluxes (Fig. 5c) correlate well with the increased stormtrack activity between 40 °N and 60 °N in TORT compared to CTRL (Fig. 6c).

3.3. The Tortonian run compared to quantitative terrestrial proxy data

Steppuhn et al. (2007) established a method of comparing model results and quantitative terrestrial proxy data. In order to evaluate the

model performance, we apply this method to the mean annual temperature (MAT) and mean annual precipitation (MAP) of TORT. Steppuhn et al. (2007) present a compilation of quantitative proxy data for the Tortonian (11 to 7 Ma). Based on the palaeobotanical record that was surveyed within the frame of NECLIME, we update this dataset with results from recently published studies (Akgün et al., 2007; Bruch et al., 2007; Utescher et al., 2007; Liu et al., 2011-this issue; Yao et al., 2011-this issue), and we add the study of Wolfe et al. (1997). We also complete the dataset with estimates of annual precipitation using large mammal hypsodonty, i.e. the relationship between mean tooth crown height of fossil mammals and annual precipitation (Fortelius et al., 2002; Eronen et al., 2010a). We use data from Eronen et al. (2010b). From this dataset we use only those localities which are dated between MN9 and MN12 in the European mammal units (Steininger et al., 1996; Steininger, 1999).

The dataset used in the present study now comprises in total 433 localities. Therein, 111 sites provide palaeobotanical information about MAT, and 423 sites (319 large mammal data) about MAP. Climate reconstructions for mean annual temperature and annual precipitation usually represent climatic ranges from a minimum to a maximum value. Following Steppuhn et al. (2007), we construct similar ranges using the minimum and maximum of mean annual temperature and precipitation from our 10-year timeseries of TORT. We then compare the climate ranges of model and proxy data. If both climate intervals overlap, we define model results and proxy data as consistent (i.e., the difference equals zero). If, however, both intervals do not overlap, the measure of inconsistency is equal to the smallest distance between the intervals. Fig. 7 represents the comparison of TORT against proxy data.

For mean annual temperatures (Fig. 7a), the agreement between TORT and proxy data is quite good. The model tends to be too cool only for some few localities. Proxy data suggest warmer conditions than the model in Alaska (−2.7 °C), eastern Siberia (−7.7 °C), in Tibet (−8.1 °C), and for parts of Europe. Contrarily, the model is too warm compared to proxy data for sites in southern China (up to +10 °C in maximum) and single localities in Africa (+4.2 °C) and New Guinea (+3.4 °C). Hence, the model-proxy comparison indicates too warm conditions in tropical to subtropical latitudes, while higher latitudes around the northern Pacific Ocean seem to be too cool in TORT. For some sites in western North America, mean annual temperatures agree with the model results as well as other localities from Tibet show consistency. Moreover, TORT demonstrates an overall good performance for Europe. Very few Central European localities tend to be about −2 °C too cool in TORT. In the Eastern Mediterranean the model is a bit warmer (about +2.5 °C) than proxy data. Altogether, there is a fairly good agreement for mean annual temperatures between TORT and quantitative terrestrial proxy data.

For annual precipitation (Fig. 7b), the consistency between model and proxy data is also generally good. Single localities in South America and Australia indicate consistent results in TORT compared to NOW proxy data. The model gives higher precipitation in tropical South-East Asia (about +1000 mm/a). For some sites in the more western part of Asia, TORT tends to slightly underestimate annual rainfall compared to large mammal data. In the European realm, we observe some differences in precipitation (Fig. 7b) between the Tortonian model run and proxy data. TORT and proxy data indicate good agreement in rainfall in Central Europe. In the western Mediterranean, the model experiment indicates increased aridity, even though some fossil sites with palaeobotanical data suggest higher annual precipitation rates than today. Around the eastern Mediterranean, we observe that the Tortonian run underestimates annual precipitation for several localities. These discrepancies in TORT occur in the comparison with both palaeobotanical and large mammal data. In contrast, to this discrepancy between proxy data and TORT concerning the Eastern Mediterranean and the south-western Eastern

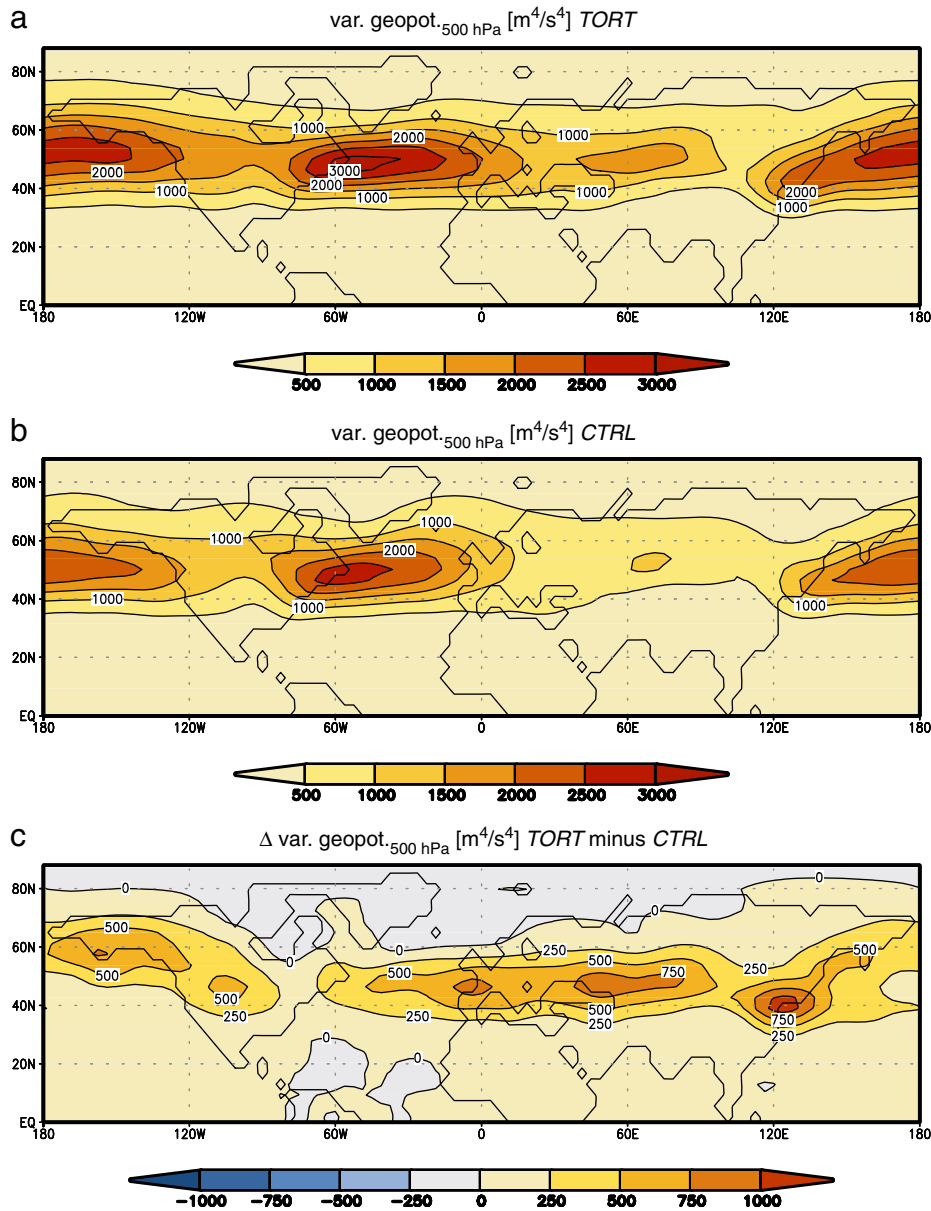


Fig. 6. The variance of the band-pass filtered geopotential at 500 hPa (in m^4/s^4) for a) the Tortonian run, b) the present-day control run, and c) the differences between the Tortonian and the present-day control run.

Paratethys, the sedimentological features fit well to the model scenario. Oolite shoals become ubiquitous during the Tortonian (= Bessarabian in regional stratigraphy) from eastern Romania to Crimea suggesting low precipitation (Munteanu and Munteanu, 1997). Evidence correlating to the late Sarmatian (Böhme et al., 2008) and the Tortonian (Eronen et al., 2009) also support dry conditions in the E-Mediterranean and E-Paratethys region. However, the general agreement of TORT with proxy-based rainfall estimates is fairly good. In terms of temperature and precipitation, Western and Central Europe in TORT agree better with proxy data, while contrarily South-Eastern Europe indicates a trend towards slightly too warm conditions and a trend towards underestimated rainfall.

4. Discussion

4.1. Global perspective on model results

We perform a climate modelling experiment for the Tortonian with the AOGCM COSMOS. The Tortonian simulation is $+1.5^\circ\text{C}$

warmer than today and global precipitation increases by $+43\text{ mm/a}$. The previous version of the AGCM ECHAM4 was applied to the Tortonian using basically the same boundary conditions (cf. above), but the AGCM was coupled to a slab ocean model (Steppuhn et al., 2006, 2007; Micheels et al., 2007). Compared to our results, the Tortonian model run of Micheels et al. (2007) demonstrated a weaker warming ($+0.6^\circ\text{C}$) and a weaker increase in global precipitation ($+26\text{ mm/a}$). For the Middle Miocene using a comparable model configuration, Tong et al. (2009) obtained similar results ($+0.6^\circ\text{C}$ and $+27\text{ mm/a}$) as Micheels et al. (2007). A Late Miocene climate modelling sensitivity study with a simple AGCM coupled to a slab ocean model demonstrated a global temperature difference of $+2.3^\circ\text{C}$ compared to a present-day experiment (Micheels et al., 2009b). Hence, Miocene experiments with AGCMs coupled to slab ocean models (Micheels et al., 2007, 2009b; Tong et al., 2009) generally show a more moderate warming compared to our experiment with a fully-coupled AOGCM. These kinds of differences were also observed from Pliocene modelling studies. An experiment for the mid-Pliocene warm period with a coupled AOGCM

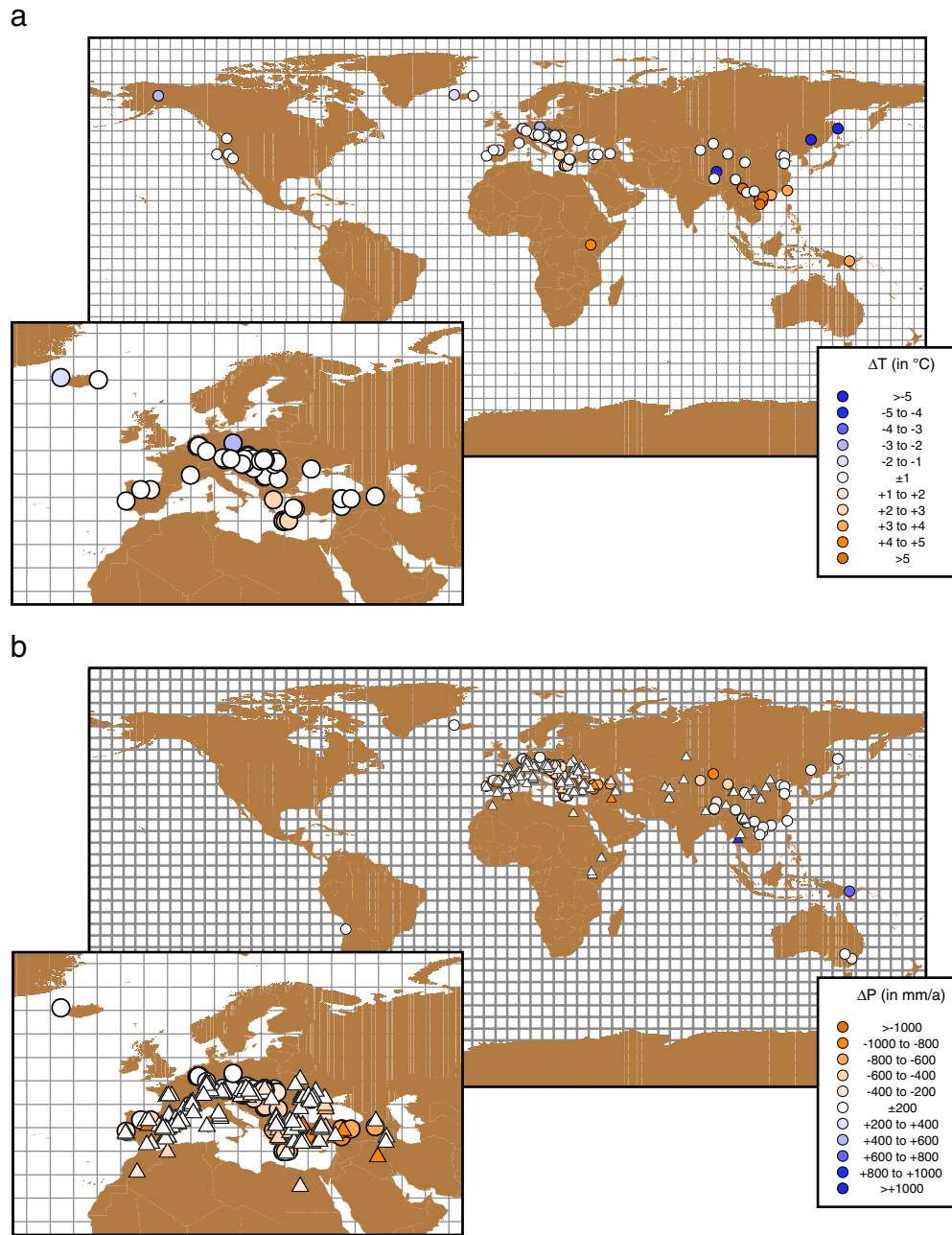


Fig. 7. The differences between the Tortonian run and terrestrial proxy data for a) the mean annual temperature (in °C), and b) the annual precipitation (in mm/a). Europe is shown enlarged. The circles represent data using various (mostly palaeobotanical) reconstruction methods, and the triangles represent data based on large mammal hypsodonty.

demonstrated a global average temperature of 18.3 °C (Haywood and Valdes, 2004), which is very close to TORT (18.0 °C). In case of using an AGCM with fixed Pliocene sea surface temperatures, the Pliocene experiment was still warmer than present (+1.6 °C), but compared to the coupled model configuration (+3.1 °C) the warming was less pronounced (Haywood and Valdes, 2004; Haywood et al., 2009). Our results for the Tortonian presented here are within the range of previous Middle Miocene to mid-Pliocene experiments, but the usage of different models and their configurations limit the comparability of results. Therefore, it is useful to consider the fossil record for evaluating the reliability of our results.

We compare mean annual temperatures and annual precipitation of TORT with terrestrial proxy data (Fig. 7). The consistency of TORT and proxy data is better than for previous Tortonian experiments with ECHAM4/ML (Micheels et al., 2007; Steppuhn et al., 2007). The model–proxy data comparison demonstrates a generally good

agreement also in the North Atlantic and European realm. Hence, the Tortonian experiment represents fairly well the warm Late Miocene conditions in mid- to higher latitudes. Moreover, previous experiments were unable to produce sufficiently warm conditions in high latitudes (Micheels et al., 2007). This is improved in TORT, even though some discrepancies in Eastern Siberia and Alaska still remain. TORT represents a largely reduced Arctic sea ice volume. When the glaciation of the Northern Hemisphere had started still is a debate (e.g., Moran et al., 2006, and references therein). Data from ocean drilling recently indicated that there has been sea ice cover since Eocene times (e.g., Brinkhuis et al., 2006; Moran et al., 2006; Stickley et al., 2009). During much of the Miocene the Arctic was covered by perennial sea ice, but increased abundances of dinoflagellates at ~8 Ma and ~9 Ma hint at seasonal sea ice cover (Moran et al., 2006). Our Tortonian model experiment supports rather more the persistent sea ice cover of the Arctic than seasonally ice-free conditions. In

addition, the model–proxy data comparison (Fig. 7) demonstrates a good agreement in the North Atlantic and European realm. Hence, the Tortonian experiment represents fairly well the warm Late Miocene conditions in the mid- to high latitudes.

4.2. Weak points in the model experiment

In order to test the robustness of results of our Tortonian run, we performed a quantitative comparison with proxy data (Fig. 7). The consistency between model results and proxy data is fairly good, but still there are some shortcomings. These differences can be attributed to the model including its setup and/or to proxy data. The COSMOS model includes some parameterisations (e.g., cloud physics). Per definition parameterisations are simplified schemes of some physical processes and include uncertainties. However, the AGCM ECHAM5 and the OGCM MPIOM are well-tested (Giorgetta et al., 2006, and references therein) and the model physics should not explain differences of TORT compared to proxy data. We observe discrepancies in the Tortonian experiment, which can be attributed to weak points in the boundary conditions. The model resolution is too coarse to represent small-scale details of the palaeogeography and -orography, but the most important features should be included in TORT. Moreover, reconstructions of palaeoelevations and -depths are difficult and related to uncertainties. For example, the uplift of the Tibetan Plateau is still discussed controversially and, hence, the palaeoelevation is not fully clear (e.g., Molnar, 2005, and references therein; Spicer et al., 2003). Some evidences support that southern Tibet was as high as today since the Middle Miocene (Spicer et al., 2003), but the mean elevation of Tibet was lower (Molnar, 2005). Consistent to previous Tortonian experiments (e.g., Micheels et al., 2007, 2009a,b) and other studies (e.g., Ramstein et al., 1997; Lunt et al., 2008), TORT represents a reduced palaeoelevation of Tibet. The open Panama Strait and the Paratethys are also sources of uncertainties in TORT. In the Middle Miocene, the depth of the Panama Isthmus was about 1000 metres (e.g., Duque-Caro, 1990; Herold et al., 2008). At around 3 Ma, there was the final closure of the Central American Isthmus (Haug and Tiedemann, 1998; Bartoli et al., 2005). Some studies suggest a temporary closure of the Panama Isthmus already in the Early Tortonian (e.g., Kameo and Sato, 2000; Roth et al., 2000). Representing the Tortonian as an average situation over a time span of 4 Ma and considering that the final closure occurred in the Pliocene, we assume an open seaway as a mean condition. Based on Collins et al. (1996), we assume a depth of 500 metres for the Central American Isthmus, but it could have been shallower (Collins et al., 1996). With a depth of 200 metres (Collins et al., 1996), the poleward heat transport in the North Atlantic would still be weaker than present but more intense than in TORT. Moreover, this can explain why our AOGCM experiment represents greater warming than previous Tortonian model experiments with ECHAM4 coupled to a mixed-layer model (Steppuhn et al., 2006; Micheels et al., 2007). The OHT in TORT is reduced by -0.5 PW (Fig. 5a) and equatorial regions are about $+1$ °C warmer than in CTRL (Fig. 3a). Experiments with ECHAM4/ML prescribed an ocean heat transport, which was only -0.2 PW weaker than present (Steppuhn et al., 2006), and low latitudes were about $+0.5$ °C warmer compared to today (Micheels et al., 2007). A less reduced ocean heat transport (e.g., due to a shallower Central American Isthmus) provides a mechanism for cooler tropics than in TORT. Further sensitivity studies are needed to fully address the climatic consequences of changes of the depth of the Central American Isthmus during Miocene. Concerning the Paratethys, our reconstruction might also include some shortcomings, but it is largely consistent to other studies (e.g., Popov et al., 2004; Herold et al., 2008). Previous Tortonian experiments did not include the Paratethys (Steppuhn et al., 2006, 2007; Micheels et al., 2007). In TORT, we now consider this source of latent heat in the atmosphere, which is an important feature for the Neogene climate (Ramstein et al., 1997).

Finally, we set the carbon dioxide concentration to 360 ppm in TORT, which is also used in the present-day reference experiment. For the Miocene, various and diverging estimations for atmospheric $p\text{CO}_2$ exist (e.g., Cerling, 1991; MacFadden, 2005; Pagani et al., 2005; Kürschner et al., 2008). Depending on the different methods, CO_2 might have been lower than 300 ppm (e.g., Pagani et al., 2005) or higher than 500 ppm (e.g., Cerling, 1991; MacFadden, 2005). Taking these divergent estimations into account, the present-day CO_2 level is also reasonable for the Late Miocene. As a whole, the Tortonian model configuration is consistent to previous studies (e.g., Micheels et al., 2007) and it represents the major characteristics. At least in terms of a sensitivity experiment, we are confident to rely on our results. The comparison to proxy data also demonstrates a good performance of the model simulation.

4.3. Weak points in the proxy data

The comparison of model results and proxy data is difficult mainly by two factors. On the one hand, the Tortonian run with its boundary conditions is designed as a time-average. In contrast, proxy data usually represent stratigraphic snapshots. Hence, there are pseudo-discrepancies because short-lived conditions shown in the fossil record cannot be represented in TORT. For instance, Böhme et al. (2008) suggest variable precipitation in Southwest and Central Europe with significantly wetter (“washhouse”) conditions and drier periods in the Middle and Late Miocene. The model cannot represent the variability between more humid and drier periods in the Late Miocene, but on average over the time span of 4 Ma TORT supports the relatively wet climate in Central Europe. The age of localities can also include uncertainties. Localities from the S-German Molasse Basin commonly attributed to the Tortonian might have an older age (Böhme, pers. comm.). If these sites belong to the late Serravallian, this would explain some discrepancies between TORT and proxy data. For Iceland, we use two localities with a slightly different age, but both still refer to the Tortonian (Micheels et al., 2007). Considering that climate was not constant during the Tortonian, the different age of both localities can explain why one site is consistent and the other is inconsistent in the model run compared to proxy data (Fig. 7a). On the other hand, the global climate model resolves the regional scale, whereas proxy data are local pinpoints. In mountainous areas such as Tibet, the model can represent more the larger-scale rainfall trend and proxy data resolve local conditions. Even though these facts explain some discrepancies, they also offer the possibility to combine the different techniques to better understand the environmental context and the processes related to climatic changes within shorter time intervals (e.g., Eronen et al., 2009; Micheels et al., 2009a). In addition to these explanations, the geological setting is also a methodologically inherent bias. Proxy data are more frequently obtained from limnic, fluvial or coastal marine sites, while non-aquatic continental sections are rare. This can lead to an unbalanced ration between locally wet and dry signals. Furthermore, climate reconstructions can fail for parameters, which are not limiting factors. For instance, animals and vegetation depend on water availability. If fluvial systems provide enough water, animals and vegetation should be (more or less) independent from the amount of annual rainfall. The major part of the floras studied represent lowland sites in depositional centres, where availability of groundwater certainly played an important role. Thus, plant based data potentially overestimate precipitation (Utescher et al., 2000). Similarly, mean annual temperature in tropical/subtropical zones might not be a limiting factor as long as throughout the year temperatures do not fall below a certain threshold. For example, this would explain temperature differences between TORT and proxy data in SE-China (Fig. 7a). Some studies demonstrated that climate reconstructions based on different techniques do not give a fully coherent picture of the past (e.g., Uhl et al., 2007). Nevertheless, the quality of the sum of all proxy data used in our study is reliable.

4.4. Atmosphere and ocean heat transport

The major aim of this study is to understand the heat transport in the Late Miocene compared to today. These mechanisms were not so frequently addressed, but they are a key for understanding the warm Miocene climate. From our Tortonian run, we observe that there is more energy in the Earth's system (Fig. 3b). In the Arctic region, the Late Miocene boreal forests and the absence of the Greenland ice sheet lead to a higher energy input (albedo effect) compared to today, but primarily tropics and subtropics show a higher energy input. These differences in the energy balance need to modify the heat transport mechanisms (Fig. 5) as well as boundary conditions like the open Central American Isthmus induce changes. The open Panama Strait in TORT reduces the ocean heat transport and the atmosphere tries to compensate. In fact, the total atmospheric heat transport in mid-latitudes tends to be even less than today. However, this is just because of a decreased potential energy flux with the mean meridional circulation. The reduced heat transport in the North Atlantic leads to a cooling effect in the European realm (Fig. 4a). The increased atmospheric sensible heat flux (Fig. 8b) partly buffers the cooling effect. In addition, the moisture flux from the Atlantic Ocean towards Europe increases in TORT (Figs. 4b, 8c). Transient eddies manage the increased poleward transport of sensible and latent heat (Fig. 5c). The more efficient transient eddy heat flux is equivalent to the more frequent/intense storms represented in the northern mid-latitudes (Fig. 6).

It is difficult to compare our results for the heat transport with others because Miocene and Pliocene modelling studies have not addressed these mechanisms so much in detail. Consistent to ocean modelling experiments, which focussed on the effects of the opening and closure of ocean gateways during the Cenozoic (e.g., Mikolajewicz and Crowley, 1997; Bice et al., 2000), we observe a weaker northward ocean heat transport. In an OGCM sensitivity experiment with a deeply opened Panama Isthmus (2700 meters), the global ocean heat transport decreases by -0.7 PW (Maier-Reimer et al., 1990). Taking into account that the Central American Isthmus is much deeper than in our scenario, this study basically agrees with our results. Compensating for the weak ocean in TORT, the total atmospheric heat transport increases with up to $+1$ PW compared to the reference run (cf. Fig. 5a). In a mid-Pliocene model experiment using a fully-coupled AOGCM, the maximum northward ocean heat transport is $+0.2$ PW stronger than today and the atmospheric response (-0.3 PW in the tropics) is in the same order of magnitude (Haywood and Valdes, 2004). It is the question how much is hidden behind this weak atmospheric change in terms of the sensible, potential and latent heat fluxes, respectively. Micheels et al. (2009a) demonstrated that the appearance of the Sahara desert compared to grassland in the Late Miocene led to a decrease of more than -1 PW in the sensible northward heat flux and of -0.5 PW in the latent northward heat flux in equatorial regions. Although less pronounced, these trends are represented in TORT. On the one hand, the study of Micheels et al. (2009a) was designed as a specific sensitivity experiment to figure out the climatic effects of the Sahara. On the other hand, we here apply a complex AOGCM, whereas Micheels et al. (2009a) used a simple AGCM coupled to a slab ocean model. The representation of the ocean is more realistic in our Tortonian run also because Micheels et al. (2009a) specified a present-day flux correction for their Late Miocene experiment.

4.5. North Atlantic and European Region

In the Tortonian model run, the reduced heat transport in the North Atlantic Ocean is levelled out by an increased atmospheric heat transport. Associated with the more intense stormtrack, strengthened westerlies in TORT (Fig. 8a) increase the moisture transport (Fig. 8c) from the Atlantic Ocean onto the European continent. As a result of the increased latent heat transport, precipitation in TORT is higher than at present in the northern and easternmost parts of Europe.

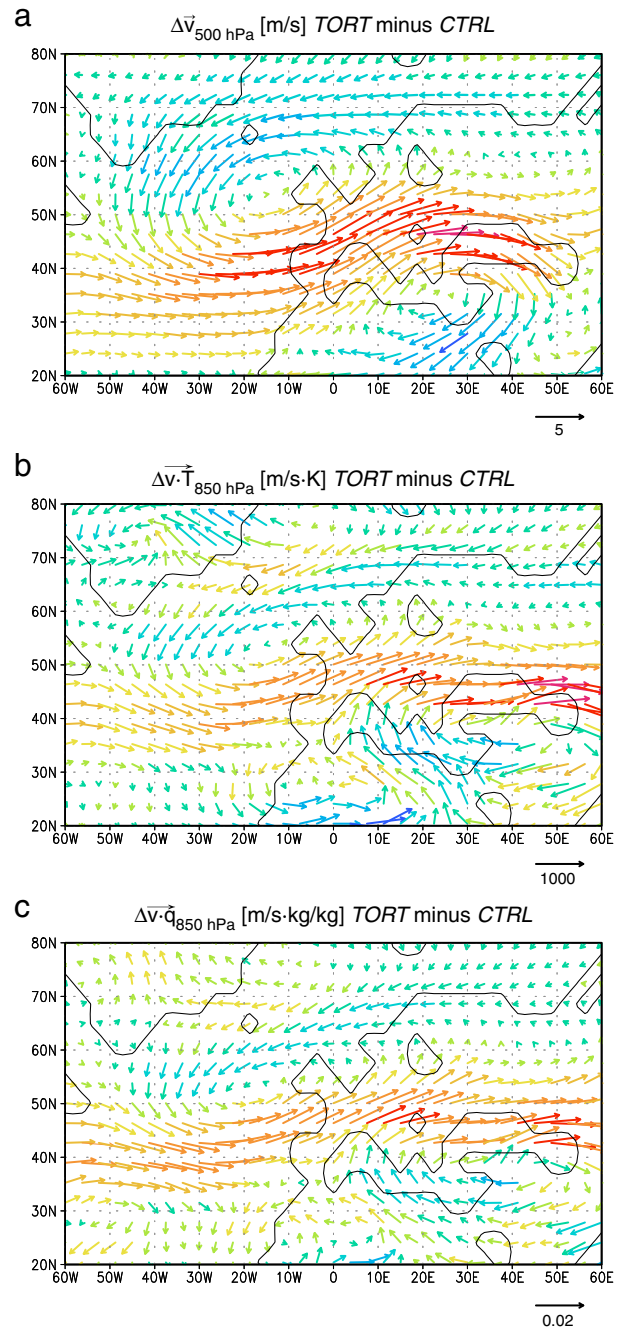


Fig. 8. The annual average differences of a) the wind field at 500 hPa (in m/s), b) the sensible heat flux at 850 hPa (m/s K), and c) the latent heat flux at 850 hPa (m/s kg/kg) between the Tortonian run and the present-day control run for the North Atlantic/European region. The reference arrow represents 5 m/s in a, 1000 m/s K in b, and m/s kg/kg in c; colour coding indicates differences of magnitudes (red = increase, blue = decrease) between the Tortonian and the present-day control run.

Consistently, palaeontological data point to humid conditions in most parts of Europe except for the south-east (e.g., Mosbrugger et al., 2005; Bruch et al., 2007). Palaeobotanical MAP data range from 700 to 1400 mm with a slight geographical trend to lower values in southern regions of Europe (Bruch et al., 2007). These values are equivalent to a positive precipitation anomaly of $+0.5$ to $+2$ mm/day with respect to modern conditions. These anomalies tend to be more pronounced than simulated in TORT compared to CTRL (Fig. 4b), but both spatial patterns agree fairly well with each other.

The causes of climatic anomalies between TORT and CTRL in Europe are mostly a result of differences in atmospheric circulation as a

response on the weak ocean heat transport. A Tortonian $\delta^{18}\text{O}$ -record from Crete indicated seasonal and interannual climate variability on time scales similar to the modern patterns of the North Atlantic Oscillation (Brachert et al., 2006). Therefore, Brachert et al. (2006) concluded that the E-Mediterranean in the Late Miocene was linked to climate variability in the North Atlantic region. We observe a pattern from Fig. 8, which resembles the atmospheric flow for modern positive mode of the North Atlantic Oscillation during the winter season. However, it is an annual mode in case of the Tortonian run. Eronen et al. (2009) investigated the change of the Pikermian chronofauna on the much longer time-scale from 12 to 4.2 Ma. In the latest Middle Miocene (~12 Ma) and in the Early Pliocene (~4 Ma), more humid conditions prevailed in the E-Mediterranean region, while for 8 to 7 Ma the faunal record showed aridity (Eronen et al., 2009). This long-term trend can be associated with changes in the North Atlantic region (Figs. 6 and 8) due to the open Central American Isthmus and the absence of a Greenland ice sheet in the Miocene (cf. also Brachert et al., 2006) with their influence on atmospheric circulation.

4.6. The monsoon system in Asia

GCM studies repeatedly focussed on the uplift of the Tibetan Plateau as the major trigger for the evolution of the Asian monsoon (e.g., Ramstein et al., 1997; Fluteau et al., 1999; Liu and Yin, 2002; Zhang et al., 2007). The retreat of the Paratethys was also a factor, which influenced the monsoon (e.g., Fluteau et al., 1999; Zhang et al., 2007). Geological evidences support a weak Late Miocene monsoon system in Asia (e.g., An et al., 2001; Sun and Wang, 2006). Consistent to the fossil record, the E-Asian monsoon precipitation is weaker than present in TORT due to the low elevation of Tibet, but rainfalls strongly increase in India (cf. Fig. 4b). The warmer-than-present Indian Ocean (cf. Fig. 4a) provides an increased amount of moisture, which is transported towards India and leads to higher rainfall rates over the Indian Ocean the Indian subcontinent. Previous model experiments using a modern ocean setup did not represent an intensified Indian monsoon (e.g., Fluteau et al., 1999; Liu and Yin, 2002; Zhang et al., 2007). Moreover, TORT compared to CTRL indicates that the intensification of the E-Asian monsoon can have been linked to a weakening of the Indian monsoon rainfall. The monsoon in E-Asia intensified at the end of the Miocene towards the Pliocene (An et al., 2001; Guo et al., 2004). Generally, interior parts of Asia became more arid during the evolution of the monsoon (An et al., 2001; Guo et al., 2004). This trend is represented in the Tortonian experiment.

The uplift of Tibet is not the only factor, which influences the monsoon system. Based on the present-day observation dataset ERA-40, Bothe et al. (2009) claimed a linkage of the monsoon in Asia to conditions in the N-Atlantic/European region. Recent drought conditions in Tibet are associated with higher pressure in Scandinavia and Atlantic stormtracks are more from the SW to NE (Bothe et al., 2009). Tibet is contrarily wet, if stormtracks have a more zonal orientation related to lower pressure in Central Europe (Bothe et al., 2009). Our model experiment represents the key features of this wet Tibet-scenario. The stormtrack system in the North Atlantic region intensifies in TORT (Fig. 6), and it has a more zonally orientated character (Figs. 6 and 8). This is comparable to Bothe et al. (2009). Directly for Tibet, precipitation does not change very much in TORT. However, the Tibetan Plateau is in the transitional zone in between the more humid Indian subcontinent and the more arid parts of E-Asia. Consistent to our modelling study, Bothe et al. (2009) observed an increased moisture flux from the Gulf of Bengal towards India (cf. Fig. 4b).

5. Summary and conclusions

The understanding of warm high latitudes in the Late Miocene is not complete. We performed a model simulation for the Tortonian using the AOGCM COSMOS to address changes in the differences in

heat transport mechanisms to modern conditions. The main results of our study are that there is more energy trapped in the Tortonian Earth's system, which needs to be distributed over the globe. Moreover, the ocean heat transport is weaker than present because of the open Central American Isthmus. In case of our Tortonian experiment, the atmosphere compensates for the reduced poleward ocean heat transport. In northern mid-latitudes, the total northward atmospheric heat transport tends to be reduced compared to today. Mostly, this can be attributed to reductions in the potential heat flux with the mean meridional circulation. The transient eddy heat transport, however, increases in the palaeoclimate simulation, which is associated with intensified stormtracks in mid-latitudes. Thus, more frequent and more intense storms transport sensible and latent heat towards the pole in the Late Miocene run. This increased heat transport leads to warmer conditions in higher latitudes and, hence, generates a weaker-than-present meridional temperature gradient.

When comparing model results with quantitative terrestrial proxy data, we observe some discrepancies for some specific localities. However, the large patterns in our Tortonian run agree fairly well with the fossil record. Moreover, proxy data suggested more humid conditions in Northern and Central Europe than today. Based on the analysis of the heat transport, the model consistently supports that increased humidity in Europe is related to the intensified stormtracks, which transport more moisture from the Atlantic Ocean towards Europe. Nevertheless, detailed studies are needed to analyse inconsistencies between proxy data obtained from various data sets and with different methods. This should include a careful evaluation of the quality and reliability of proxy data, especially in cases where model data and proxies are contradictory. Future work will address a more sophisticated comparison of model results and proxy data. The present NECLIME special issue focussed on the terrestrial domain and atmospheric patterns. The ocean was beyond our scope, but it is relevant for the understanding of the Cenozoic climate cooling. We aim at a detailed analysis of the ocean modelling results for a separate forthcoming manuscript, which will also include marine proxy data to evaluate the reliability of our Tortonian experiment.

Acknowledgements

We gratefully acknowledge the comments of our two anonymous reviewers, which helped to improve our manuscript. The present work is a contribution to the NECLIME framework. It was financially supported by the Deutsche Forschungsgemeinschaft DFG within the project FOR 1070 and the federal state Hessen (Germany) within the LOEWE initiative. We also acknowledge financial support from the Kone foundation and the Academy of Finland. The modelling work was supported by CoMS grant from the Finnish Funding Agency for Technology and Innovation. The COSMOS model was provided by the Max Planck Institute for Meteorology in Hamburg (Germany). Model experiments were performed at CSC in Espoo (Finland) with special technical support from Juha Lento.

References

- Akgün, F., Kayseri, M.S., Akkiraz, M.S., 2007. Palaeoclimatic evolution and vegetational changes during the Late Oligocene–Miocene period in Western and Central Anatolia (Turkey). *Palaeogeography, Palaeoclimatology, Palaeoecology* 253, 56–90.
- An, Z., Kutzbach, J.E., Prell, W.L., Porter, S.C., 2001. Evolution of Asian monsoons and phased uplift of the Himalaya–Tibetan plateau since Late Miocene times. *Nature* 411, 62–66.
- Bartoli, G., Sarnthein, M., Weinelt, M., Erlenkeuser, H., Garbe-Schönberg, D., Lea, D.W., 2005. Final closure of Panama and the onset of northern hemisphere glaciation. *Earth and Planetary Science Letters* 237, 33–44.
- Bice, K.L., Scotese, C.R., Seidov, D., Barron, E.J., 2000. Quantifying the role of geographic change in Cenozoic ocean heat transport using uncoupled atmosphere and ocean models. *Palaeogeography, Palaeoclimatology, Palaeoecology* 161, 295–310.
- Böhme, M., Ilg, A., Winkhofer, M., 2008. Late Miocene “washhouse” climate in Europe. *Earth and Planetary Science Letters* 275, 393–401.

- Bothe, O., Fraedrich, K., Zhu, X., 2009. The large-scale circulations and summer drought and wetness on the Tibetan plateau. *International Journal of Climatology* 30, 844–855. doi:10.1002/joc.1946.
- Brachert, T.C., Reuter, M., Felis, T., Kroeger, K.F., Lohmann, G., Micheels, A., Fassoulas, C., 2006. Late Miocene corals (10 Ma) document interannual climate variability controlled by the Icelandic Low (Crete, Greece). *Earth and Planetary Science Letters* 245, 81–94.
- Brinkhuis, H., Schouten, S., Collinson, M.E., Sluvis, A., Sinninghe Damste, J.S., Dickens, G. R., Huber, M., Cronin, T.M., Onodera, J., Takahashi, K., Bujak, J.P., Stein, R., van der Burgh, J., Eldrett, J.S., Harding, I.C., Lotter, A.F., Sangiorgi, F., Konijnburg-vanCittert, H., de Leeuw, J.W., Matthiessen, J., Backman, J., Moran, K., Expedition 302 Scientists, 2006. Episodic fresh surface waters in the Eocene Arctic Ocean. *Nature* 441, 606–609.
- Bruch, A.A., Uhl, D., Mosbrugger, V., 2007. Miocene climate in Europe – patterns and evolution: a first synthesis of NECLIME. *Palaeogeography, Palaeoclimatology, Palaeoecology* 253, 1–7.
- Cerling, T.E., 1991. Carbon dioxide in the atmosphere: evidence from Cenozoic and Mesozoic palaeosols. *American Journal of Science* 291, 377–400.
- Collins, L.S., Coates, A.G., Berggren, W.A., Aubry, M.-P., Zhang, J., 1996. The late Miocene Panama isthmian strait. *Geology* 24, 687–690.
- Crowley, T.J., 2000. Carbon dioxide and Phanerozoic climate. In: Huber, B.T., MacLeod, K.G., Wing, S.L. (Eds.), *Warm Climates in Earth History*. Cambridge University Press, Cambridge, p. 462.
- Dowsett, H.J., 2007. The PRISM palaeoclimate reconstruction and Pliocene sea-surface temperatures. In: Williams, M., Haywood, A.M., Gregory, F.J., Schmidt, D.N. (Eds.), *Deep-Time Perspectives on Climate Change: Marrying the Signal from Computer Models and Biological Proxies*. The Micropalaeontological Society, Special Publications, The Geological Society, London, pp. 459–480.
- Duque-Caro, H., 1990. Neogene stratigraphy, paleoceanography and paleobiogeography in northwest South America and the evolution of the Panama seaway. *Palaeogeography, Palaeoclimatology, Palaeoecology* 77, 203–234.
- Dutton, J.F., Barron, E.J., 1997. Miocene to present vegetation changes: a possible piece of the Cenozoic puzzle. *Geology* 25 (1), 39–41.
- Eronen, J.T., Mirzaie, M., Karne, A., Micheels, A., Bernor, R.L., Fortelius, M., 2009. Distribution history and climatic controls of the Late Miocene Pikermian chronofauna. *Proceedings of the National Academy of Sciences USA* 106, 11,867–11,871.
- Eronen, J.T., Puolamäki, K., Liu, L., Lintulaakso, K., Damuth, J., Janis, C., Fortelius, M., 2010a. Precipitation and large herbivorous mammals, part I: estimates from present-day communities. *Evolutionary Ecology Research* 12, 217–233.
- Eronen, J.T., Puolamäki, K., Liu, L., Lintulaakso, K., Damuth, J., Janis, C., Fortelius, M., 2010b. Precipitation and large herbivorous mammals, part II: application to fossil data. *Evolutionary Ecology Research* 12, 235–248.
- Fauquette, S., Suc, J.-P., Jimenez-Moreno, G., Favre, E., Jost, A., Micheels, A., Bachiri-Taoufiq, N., Bertini, A., Clet-Pellegrin, M., Diniz, F., Farjanel, G., Feddi, N., Zheng, Z., 2007. Latitudinal climatic gradients in Western European and Mediterranean regions from the Mid-Miocene (15 Ma) to the Mid-Pliocene (3.6 Ma) as quantified from pollen data. In: Williams, M., Haywood, A.M., Gregory, F.J., Schmidt, D.N. (Eds.), *Deep-Time Perspectives on Climate Change: Marrying the Signal from Computer Models and Biological Proxies*. The Micropalaeontological Society, Special Publications, The Geological Society, London, pp. 481–502.
- Fluteau, F., Ramstein, G., Besse, J., 1999. Simulating the evolution of the Asian and African monsoons during the past 30 Myr using an atmospheric general circulation model. *Journal of Geophysical Research* 104, 11,995–12,018.
- Fortelius, M., Eronen, J.T., Jernvall, J., Liu, L., Pushkina, D., Rinne, J., Tesakov, A., Vislobokova, I.N., Zhang, Z., Zhou, L., 2002. Fossil mammals resolve regional patterns of Eurasian climate change during 20 million years. *Evolutionary Ecology Research* 4, 1005–1016.
- Gent, P.R., Willebrand, J., McDougall, T., McWilliams, J.C., 1995. Parameterizing eddy-induced tracer transports in ocean circulation models. *Journal of Physical Oceanography* 25, 463–474.
- Giorgetta, M.A., Brasseur, G.P., Roeckner, E., Marotzke, J., 2006. Preface to special section on climate models at the Max Planck Institute for Meteorology. *Journal of Climate – Special Section* 19, 3769–3770.
- Guo, Z., Peng, S., Hao, Q., Biscaye, P.E., An, Z., Liu, T., 2004. Late Miocene–Pliocene development of Asian aridification as recorded in the Red-Earth Formation in northern China. *Global and Planetary Change* 41, 135–145.
- Hagemann, S., 2002. An Improved Land Surface Parameter Dataset for Global and Regional Climate Models. Report 336, Max-Planck-Institut für Meteorologie, Hamburg.
- Harzhauser, M., Mandic, O., 2008. Neogene lake systems of Central and South-Eastern Europe: faunal diversity, gradients and interrelations. *Palaeogeography, Palaeoclimatology, Palaeoecology* 260, 417–434.
- Harzhauser, M., Piller, W.E., 2007. Benchmark data of a changing sea. *Palaeogeography, palaeobiogeography and events in the Central Paratethys during the Miocene*. *Palaeogeography, Palaeoclimatology, Palaeoecology* 253, 8–31.
- Haug, G.H., Tiedemann, R., 1998. Effect of the formation of the Isthmus of Panama on Atlantic Ocean thermohaline circulation. *Nature* 393, 673–676.
- Haywood, A.M., Valdes, P.J., 2004. Modelling Pliocene warmth: contribution of atmosphere, oceans and cryosphere. *Earth and Planetary Science Letters* 218, 363–377.
- Haywood, A.M., Chandler, M.A., Valdes, P.J., Salzmann, U., Lunt, D.J., Dowsett, H.J., 2009. Comparison of mid-Pliocene climate predictions produced by the HadAM3 and GCMAM3 general circulation models. *Global and Planetary Change* 66, 208–224.
- Herold, N., Seton, M., Müller, R.D., You, Y., Huber, M., 2008. Middle Miocene tectonic boundary conditions for use in climate models. *Geochemistry, Geophysics, Geosystems* 9, Q10009. doi:10.1029/2008GC002046.
- Jacobs, B.F., 2004. Paleobotanical studies from tropical Africa: relevance to the evolution of forest, woodland and savannah biomes. *Philosophical Transactions of the Royal Society B* 359, 1573–1583.
- Jungclaus, J.H., Keenlyside, N., Botzet, M., Haak, H., Luo, J.-J., Latif, M., Marotzke, J., Mikolajewicz, U., Roeckner, E., 2006. Ocean circulation and tropical variability in the coupled model ECHAM5/MPI-OM. *Journal of Climate – Special Section* 19, 3952–3972.
- Kameo, K., Sato, T., 2000. Biogeography of Neogene calcareous nannofossils in the Caribbean and the eastern equatorial Pacific – floral response to the emergence of the Isthmus of Panama. *Marine Micropaleontology* 39, 201–218.
- Kuhlemann, J., 2007. Palaeogeographic and paleotopographic evolution of the Swiss and Eastern Alps since the Oligocene. *Global and Planetary Change* 58, 224–236.
- Kürschner, W.M., Kvacek, Z., Dilcher, D.L., 2008. The impact of Miocene atmospheric carbon dioxide fluctuations on climate and the evolution of terrestrial ecosystems. *Proceedings of the National Academy of Sciences USA* 105, 449–453.
- Kutzbach, J.E., Behling, P., 2004. Comparison of simulated changes of climate in Asia for two scenarios: Early Miocene to present, and present to future enhanced greenhouse. *Global and Planetary Change* 41, 157–165.
- Lawler, L.A., Gahagan, L.M., 2003. Evolution of Cenozoic seaways in the circum-Antarctic region. *Palaeogeography, Palaeoclimatology, Palaeoecology* 198, 11–37.
- Le Houerou, H.N., 1997. Climate, flora and fauna changes in the Sahara over the past 500 million years. *Journal of Arid Environments* 37, 619–647.
- Liu, X., Yin, Z.-Y., 2002. Sensitivity of East Asian monsoon climate to the uplift of the Tibetan Plateau. *Palaeogeography Palaeoclimatology Palaeoecology* 183, 223–245.
- Liu, Y.-S. (Christopher), Utescher, T., Zhou, Z., Sun, B., 2011. The evolution of Miocene climates in North China: Preliminary results of quantitative reconstructions from plant fossil records. *Palaeogeography Palaeoclimatology Palaeoecology* 304, 308–317 (this issue).
- Lunt, D.J., Flecker, R., Valdes, P.J., Salzmann, U., Gladstone, R., Haywood, A.M., 2008. A methodology for targeting palaeo proxy data acquisition: a case study for the terrestrial late Miocene. *Earth and Planetary Science Letters* 271, 53–62.
- Lyle, M., Barron, J., Bralower, T.J., Huber, M., Olivares Lyle, A., Ravelo, A.C., Rea, D.K., Wilson, P.A., 2008. Pacific Ocean and Cenozoic evolution of climate. *Reviews of Geophysics* 46 RG2002/2008..
- MacFadden, B.J., 2005. Terrestrial mammalian herbivore response to declining levels of atmospheric CO₂ during the Cenozoic: evidence from North American Fossil Horses (family Equidae). In: Ehleringer, J.R., Cerling, T.E., Dearing, M.D. (Eds.), *A History of Atmospheric CO₂ and Its Effects on Plants, Animals, and Ecosystems: Ecological Studies*, 177, pp. 273–292.
- Magyar, I., Geary, D.H., Müller, P., 1999. Palaeogeographic evolution of the Late Miocene Lake Pannon in Central Europe. *Palaeogeography, Palaeoclimatology, Palaeoecology* 147, 151–167.
- Maier-Reimer, E., Mikolajewicz, U., Crowley, T.J., 1990. Ocean general circulation model sensitivity experiment with an open Central American Isthmus. *Palaeoceanography* 5 (3), 349–366.
- Marsland, S.J., Haak, H., Jungclaus, J.H., Latif, M., Röske, F., 2003. The Max-Planck-Institute global ocean/sea ice model with orthogonal curvilinear coordinates. *Ocean Modelling* 5, 91–127.
- Meehl, G.A., Stocker, T.F., Collins, W.D., Friedlingstein, P., Gaye, A.T., Gregory, J.M., Kitoh, A., Knutti, R., Murphy, J.M., Noda, A., Raper, S.C.B., Watterston, I.G., Weaver, A.J., Zhao, Z.-C., 2007. Regional climate projections. In: Solomon, S., Qin, D., Manning, M., Chen, Z., Marquis, M., Averyt, K.B., Tignor, M., Miller, H.L. (Eds.), *Climate Change 2007: The Physical Science Basis*. Contribution of Working Group I to the Fourth Assessment Report of the Intergovernmental Panel on Climate Change. Cambridge University Press, Cambridge, pp. 747–845. United Kingdom and New York, NY, USA.
- Micheels, A., Bruch, A.A., Uhl, D., Utescher, T., Mosbrugger, V., 2007. A Late Miocene climate model simulation with ECHAM4/ML and its quantitative validation with terrestrial proxy data. *Palaeogeography Palaeoclimatology Palaeoecology* 253, 267–286.
- Micheels, A., Eronen, J., Mosbrugger, V., 2009a. The Late Miocene climate response to a modern Sahara desert. *Global and Planetary Change* 67, 193–204.
- Micheels, A., Bruch, A.A., Mosbrugger, V., 2009b. Miocene climate modelling sensitivity experiments for different CO₂ concentrations. *Palaeontologia Electronica* 12 (6A) 20 pp.
- Mikolajewicz, U., Crowley, T.J., 1997. Response of a coupled ocean/energy balance model to restricted flow through the central American isthmus. *Palaeoceanography* 12 (3), 429–441.
- Molnar, P., 2005. Mio-Pliocene growth of the Tibetan Plateau and evolution of East Asian climate. *Palaeontologia Electronica* 8 (1), 1–23 http://paleo-electronica.org/paleo/2005_1/molnar2/issue1_05.htm.
- Moran, K., Backman, J., Brinkhuis, H., Clemens, S.C., Cronin, T., Dickens, G.R., Eynaud, F., Gattacceca, J., Jakobsson, M., Jordan, R.W., Kaminski, M., King, J., Koc, N., Krylov, A., Martinez, N., Matthiessen, J., McInroy, D., Moore, T.C., Onodera, J., O'Regan, M., Pälike, H., Rea, B., Rio, D., Sakamoto, T., Smith, D.C., Stein, R., St John, K., Suto, I., Suzuki, N., Takahashi, K., Watanabe, M., Yamamoto, M., Farrell, J., Frank, M., Kubik, P., Jokat, W., Kristoffersen, Y., 2006. The Cenozoic palaeoenvironment of the Arctic Ocean. *Nature* 441, 601–605.
- Mosbrugger, V., Utescher, T., Dilcher, D.L., 2005. Cenozoic continental climatic evolution of Central Europe. *Proceedings of the National Academy of Sciences USA* 102, 14,964–14,969.
- Munteanu, E., Munteanu, M.-T., 1997. Correlation of Sarmatian deposits of the South Dobrogea and the Subcarpathians of Muntenia. *Acta Palaeontologica Romaniaica* 1, 155–159.
- Nisancioglu, K.H., Raymo, M.E., Stone, P.H., 2003. Reorganization of Miocene deep water circulation in response to the shoaling of the Central American Seaway. *Palaeoceanography* 18, 1006. doi:10.1029/2002PA000767.
- Pacanowski, R.C., Philander, S.G.H., 1981. Parameterization of vertical mixing in numerical models of tropical oceans. *Journal of Physical Oceanography* 11, 1443–1451.

- Pagani, M., Zachos, J.C., Freeman, K.H., Tipler, B., Bohaty, S., 2005. Marked decline in atmospheric carbon dioxide concentrations during the Paleogene. *Science* 309, 600–603.
- Pearson, P.N., Palmer, M.R., 2000. Atmospheric carbon dioxide concentrations over the past 60 million years. *Nature* 406, 695–699.
- Pickford, M., 2000. Crocodiles from the Beglia Formation, Middle/Late Miocene Boundary, Tunisia, and their significance for Saharan palaeoclimatology. *Annales de Paleontologie* 86 (1), 59–67.
- Popov, S.V., Rögl, F., Rozanov, A.Y., Steininger, F.F., Shcherba, I.G., Kovac, M. (Eds.), 2004. Lithological–Palaeogeographic Maps of Paratethys. 10 Maps Late Eocene to Pliocene: Courier Forschungsinstitut Senckenberg, 250, pp. 1–46.
- Ramstein, G., Fluteau, F., Besse, J., Joussaume, S., 1997. Effect of orogeny, plate motion and land–sea distribution on Eurasian climate change over past 30 million years. *Nature* 386, 788–795.
- Roekner, E., Bäuml, G., Bonaventura, L., Brokopf, R., Esch, M., Giorgetta, M., Hagemann, S., Kirchner, I., Kornbluh, L., Manzini, E., Rhodin, A., Schlese, U., Schulzweida, U., Tompkins, A., 2003. The atmospheric general circulation model ECHAM5 Part 1 – Model description. Report 349, Max-Planck-Institut für Meteorologie, Hamburg.
- Roekner, E., Brokopf, R., Esch, M., Giorgetta, M., Hagemann, S., Kornbluh, L., Manzini, E., Schlese, U., Schulzweida, U., 2006. Sensitivity of simulated climate to horizontal and vertical resolution in the ECHAM5 atmosphere model. *Journal of Climate* 19, 3771–3791.
- Rögl, F., 1998. Palaeogeographic considerations for Mediterranean and Paratethys Seaways (Oligocene to Miocene). *Annalen des Naturhistorischen Museums in Wien* 99A, 279–310.
- Roth, J.M., Droxler, A.W., Kameo, K., 2000. The Caribbean carbonate crash at the Middle to Late Miocene transition: Linkage to the establishment of the modern global ocean conveyor. In: Leckie, R.M., Sigurdsson, H., Acton, G.D., Draper, G. (Eds.), *Proceedings of the Ocean Drilling Program: Scientific Results*, 165, pp. 249–273.
- Ruddiman, W.F., Kutzbach, J.E., Prentice, I.C., 1997. Testing the climatic effects of orography and CO₂ with general circulation and biome models. In: Ruddiman, W.F. (Ed.), *Tectonic Uplift and Climate Change*. Plenum, New York, pp. 203–235.
- Senut, B., Pickford, M., Segalen, L., 2009. Neogene desertification of Africa. *C. R. Geoscience* 341, 591–602.
- Spicer, R.A., Harris, N.B.W., Widdowson, M., Herman, A.B., Guo, S., Valdes, P.J., Wolfe, J.A., Kelley, S.P., 2003. Constant elevation of southern Tibet over the past 15 million years. *Nature* 421, 622–624.
- Spiegel, C., Kuhlemann, J., Dunkl, I., Frisch, W., 2001. Paleogeography and catchment evolution in a mobile orogenic belt: the Central Alps in Oligo-Miocene times. *Tectonophysics* 341, 33–47.
- Steininger, F.F., 1999. Chronostratigraphy, Geochronology and Biochronology of the Miocene European Land Mammal Mega-Zones (ELMMZ) and the Miocene Mammal-Zones. In: Rössner, G.E., Heissig, K. (Eds.), *The Miocene Land Mammals of Europe*. Verlag Dr. Friedrich Pfeil, pp. 9–24.
- Steininger, F.F., Berggren, W.A., Kent, D.V., Bernor, R.L., Sen, S., Agustí, J., 1996. Circum-Mediterranean Neogene (Miocene–Pliocene) marine–continental chronologic correlations of European mammal units. In: Bernor, R.L., Fahlbusch, V., Mittmann, H.-W. (Eds.), *The Evolution of Western Eurasian Neogene Mammal Faunas*. Columbia University Press, New York, pp. 7–46.
- Steppuhn, A., Micheels, A., Geiger, G., Mosbrugger, V., 2006. Reconstructing the Late Miocene climate and oceanic heat flux using the AGCM ECHAM4 coupled to a mixed-layer ocean model with adjusted flux correction. *Palaeogeography, Palaeoclimatology, Palaeoecology* 238, 399–423.
- Steppuhn, A., Micheels, A., Bruch, A.A., Uhl, D., Utescher, T., Mosbrugger, V., 2007. The sensitivity of ECHAM4/ML to a double CO₂ scenario for the Late Miocene and the comparison to terrestrial proxy data. *Global and Planetary Change* 57, 189–212.
- Stewart, D.R.M., Pearson, P.N., Ditchfield, P.W., Singano, J.M., 2004. Miocene tropical Indian Ocean temperatures: evidence from three exceptionally preserved foraminiferal assemblages from Tanzania. *Journal of African Earth Sciences* 40, 173–190.
- Stickley, C.E., St. John, K., Koc, N., Jordan, R.W., Passchier, S., Pearce, R.B., Kearns, L.E., 2009. Evidence for middle Eocene Arctic sea ice from diatoms and ice-rafted debris. *Nature* 460, 376–380.
- Sun, X., Wang, P., 2006. How old is the Asian monsoon system? – Paleobotanical records from China. *Palaeogeography, Palaeoclimatology, Palaeoecology* 222, 181–222.
- Swezey, C.S., 2009. Cenozoic stratigraphy of the Sahara, Northern Africa. *Journal of African Earth Sciences* 53, 89–121.
- Tong, J.A., You, Y., Müller, R.D., Seton, M., 2009. Climate model sensitivity to atmospheric CO₂ concentrations for the Middle Miocene. *Global and Planetary Change* 67, 129–140.
- Uhl, D., Klotz, S., Traiser, C., Thiel, C., Utescher, T., Kowalski, E., Dilcher, D.L., 2007. Cenozoic paleotemperatures and leaf physiognomy – a European perspective. *Palaeogeography, Palaeoclimatology, Palaeoecology* 248, 24–31.
- Utescher, T., Mosbrugger, V., Ashraf, A.R., 2000. Terrestrial climate evolution in northwest Germany over the last 25 million years. *Palaios* 15 (5), 430–449.
- Utescher, T., Djordjevic-Milutinovic, D., Bruch, A., Mosbrugger, V., 2007. Palaeoclimate and vegetation change in Serbia during the last 30 Ma. *Palaeogeography, Palaeoclimatology, Palaeoecology* 253, 141–152.
- Utescher, T., Bruch, A.A., Micheels, A., Mosbrugger, V., Popova, S., 2011. Cenozoic climate gradients in Eurasia – a palaeo-perspective on future climate change? *Palaeogeography, Palaeoclimatology, Palaeoecology* 304, 351–358 (this issue).
- von der Heydt, A., Dijkstra, H.A., 2006. Effect of ocean gateways on the global ocean circulation in the late Oligocene and early Miocene. *Paleoceanography* 21, PA1011. doi:10.1029/2005PA001149.
- Williams, M., Haywood, A.M., Taylor, S.P., Valdes, P.J., Sellwood, B.W., Hillenbrand, C.D., 2005. Evaluating the efficacy of planktonic foraminifer calcite δ¹⁸O data for sea surface temperature reconstruction for the Late Miocene. *Geobios* 38, 843–863.
- Wolfe, J.A., 1994a. Tertiary climatic changes at middle latitudes of western North America. *Palaeogeography, Palaeoclimatology, Palaeoecology* 108, 195–205.
- Wolfe, J.A., 1994b. An analysis of Neogene climates in Beringia. *Palaeogeography, Palaeoclimatology, Palaeoecology* 108, 207–216.
- Wolfe, J.A., Schorn, H.E., Forest, C.E., Molnar, P., 1997. Paleobotanical evidence for high altitudes in Nevada during the Miocene. *Science* 276, 1672–1675.
- Wolff, J.O., Maier-Reimer, E., Legutke, S., 1997. The Hamburg Ocean Primitive Equation Model HOPE. *Deutsches Klimarechenzentrum, Hamburg, Tech.Rep.13*. 98 pp.
- Yao, Y.-F., Bruch, A.A., Mosbrugger, V., Li, C.-S., 2011. Quantitative reconstruction of Miocene climate patterns and evolution in Southern China based on plant fossils. *Palaeogeography, Palaeoclimatology, Palaeoecology* 304, 291–307 (this issue).
- You, Y., Huber, M., Müller, R.D., Poulsen, C.J., Ribbe, J., 2009. Simulation of the Middle Miocene climate optimum. *Geophysical Research Letters* 36, L04702. doi:10.1029/2008GL036571.
- Zachos, J., Pagani, M., Sloan, L., Thomas, E., Billups, K., 2001. Trends, rhythms, and aberrations in global climate 65 Ma to present. *Science* 292, 686–693.
- Zachos, J.C., Dickens, G.R., Zeebe, R.E., 2008. An early Cenozoic perspective on greenhouse warming and carbon-cycle dynamics. *Nature* 451, 279–283.
- Zhang, Z., Wang, H., Guo, Z., Jiang, D., 2007. What triggers the transition of palaeoenvironmental patterns in China, the Tibetan Plateau uplift or the Paratethys Sea retreat? *Palaeogeography, Palaeoclimatology, Palaeoecology* 245, 317–331.